NOTES AND CORRESPONDENCE

The Amplification of the ENSO Forcing over Equatorial Amazon

VASUBANDHU MISRA

Department of Meteorology, and Center for Ocean–Atmospheric Prediction Studies, The Florida State University, Tallahassee, Florida

(Manuscript received 30 September 2008, in final form 8 June 2009)

ABSTRACT

The remote influence of the El Niño–Southern Oscillation (ENSO) strongly manifests over the equatorial Amazon (EA)—including parts of southern Venezuela, Guyana, French Guiana, and Suriname—when there is a large-scale anomalous upper-level divergence over continental tropical South America. Modeling studies conducted in this paper suggest that it is because of the modulation of the local diurnal cycle of the moisture flux convergence, which results in the local amplification of the ENSO signal over the EA. Further, it is shown that the local land surface feedback plays a relatively passive but important role of maintaining these interannual precipitation anomalies over the EA region.

1. Introduction

The influence of El Niño and Southern Oscillation (ENSO) on seasonal precipitation anomalies over South America has been extensively studied (Ropelweski and Halpert 1987; Marengo 1992; Uvo et al. 1998; Grimm et al. 2000; Paegle and Mo 2002; Ronchail et al. 2002; Grimm 2003, 2004; Misra 2008a). ENSO influences the large-scale east–west and meridional circulations in the global tropics that have implications over tropical South America (Misra 2008b; Grimm 2004, 2003).

The influence of SST in tropical Atlantic SST also affects rainfall over northern South America (Enfield and Mayer 1997; Giannini et al. 2001). Rainfall over the Amazonia is also shown to have sensitivity to land surface conditions, such as vegetation and soil moisture (Marengo and Nobre 2001; Costa and Foley 2000; Misra 2008a,b). This paper is, however, focused on the seasonal precipitation anomalies from the influence of ENSO on a broad region that covers parts of equatorial Amazon, French Guiana, Suriname, Guyana, and Venezuela. This region is hereafter referred as the EA and is outlined in Fig. 1a. Given the EA's close proximity to the equator, the motivation for this paper is to understand if local processes, such as the diurnal variation, amplify the remote ENSO forcing.

2. Model description and data

a. Model description

The Center for Ocean–Land–Atmosphere Studies (COLA) coupled climate model (Misra et al. 2007; Misra and Marx 2007) is used in this study. Its atmospheric part consists of the COLA AGCM, version 3.2, at a spectral resolution of T62 with 28 sigma levels, which are identical to the National Center for Atmospheric Research–National Centers for Environmental Prediction (NCEP–NCAR) reanalysis model (Kalnay et al. 1996). The dynamical core follows from the Eulerian core of the community climate model, version 3 (Kiehl et al. 1998), wherein the dependent variables are spectrally treated except for moisture, which is advected by semi-Lagrangian scheme. The relaxed Arakawa–Schubert scheme (Moorthi and Suarez 1992; Bacmeister et al. 2000) is used for deep convective parameterization. The longwave and shortwave radiation schemes are identical to those in the Community Climate System Model, version 3 (Collins et al. 2006). The clouds are diagnosed following Slingo (1987). The cloud optical properties follow from Kiehl et al. (1998). The planetary boundary layer is a nonlocal scheme (Hong and Pan

Corresponding author address: Vasubandhu Misra, Department of Meteorology, The Florida State University, 404 Love Building, Tallahassee, FL 32306.
E-mail: vmisra@fsu.edu

DOI: 10.1175/2009JHM1108.1

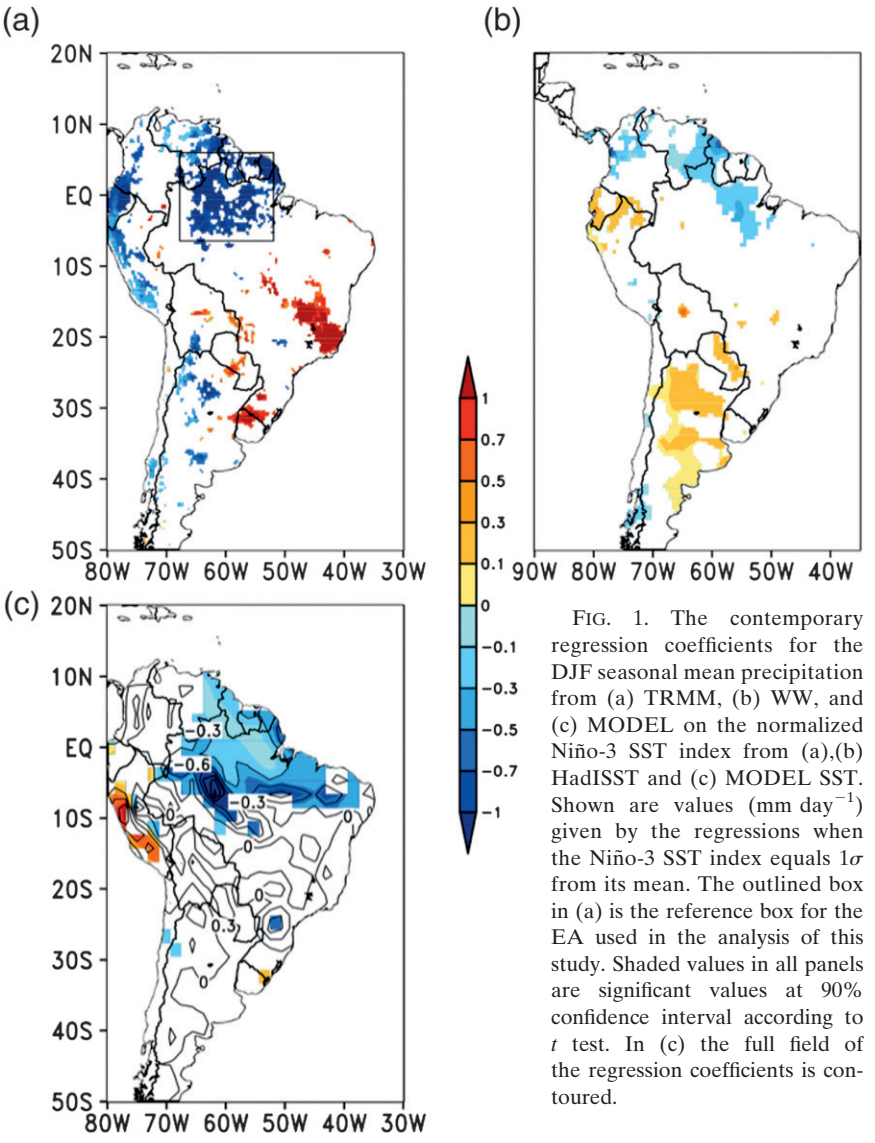

FIG. 1. The contemporary regression coefficients for the DJF seasonal mean precipitation from (a) TRMM, (b) WW, and (c) MODEL on the normalized Niño-3 SST index from (a),(b) HadISST and (c) MODEL SST. Shown are values (mm day^{-1}) given by the regressions when the Niño-3 SST index equals 1σ from its mean. The outlined box in (a) is the reference box for the EA used in the analysis of this study. Shaded values in all panels are significant values at 90% confidence interval according to *t* test. In (c) the full field of the regression coefficients is contoured.

1996), and the shallow convection uses the formulation in Tiedtke (1984). The land surface scheme uses the Simplified Simple Biosphere Model (SSiB; Xue et al. 1991, 1996; Dirmeyer and Zeng 1999). It may be noted that the COLA coupled climate model does not include variations in the greenhouse gases, solar variability, volcanoes, and aerosols.

This COLA AGCM is coupled to the Modular Ocean Model, version 3 (MOM3; Pacanowski and Griffies 1998). MOM3 covers the global oceans between 74°S and 65°N with realistic bottom topography. However, ocean depths less than 100 m are set to 100 m, and the maximum depth is set to 6000 m. The artificial high-latitude meridional boundaries are impermeable and insulating. It has a uniform zonal resolution of 1.5°, whereas the meridional grid spacing is 0.5° between 10°S and 10°N, gradually increasing to 1.5° at 30°N and 30°S, and fixed at 1.5° in the extratropics. The vertical mixing is the nonlocal *K*-profile parameterization of Large et al. (1994). The momentum mixing is the space–time dependent scheme of Smagorinsky (1963), tracer-mixing follows Redi (1982), and Gent and McWilliams (1990) is used for quasi-adiabatic stirring.

b. Data

The COLA coupled climate model was integrated for a period of 100 years from a well spun-up ocean initial condition that were obtained from a previous multi-decadal coupled integration from the same coupled model. However, the results are presented from the last

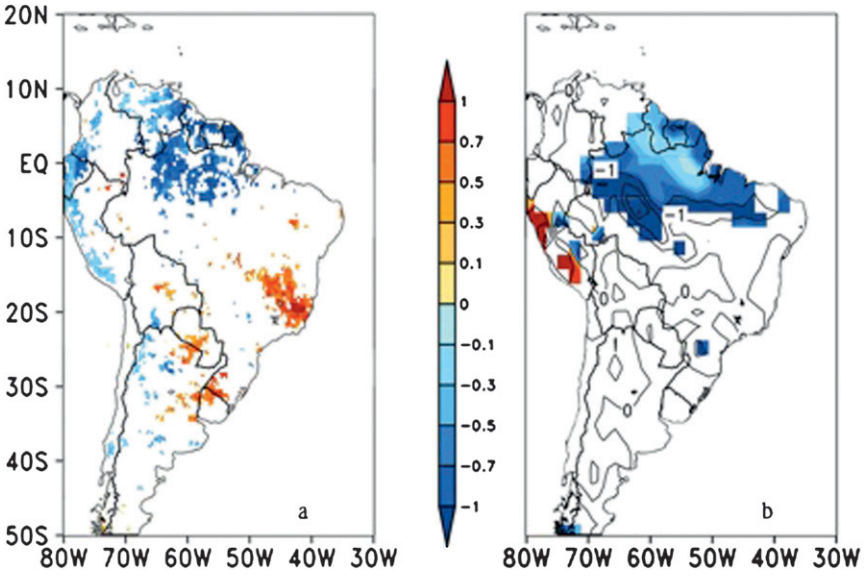

FIG. 2. The contemporary regression coefficients for the DJF seasonal mean daily diurnal precipitation range from (a) TRMM and (b) MODEL on the normalized Niño-3 SST index from (a) HADISST and (b) MODEL SST. Shown are values given by the regressions when the Niño-3 SST index equals 1σ from its mean. The units are in mm day^{-1}. In (a), the regression coefficients are scaled by a factor of 4 to use the same contour interval as (b). Shaded values in the two panels are significant values at 90% confidence interval according to t test. In (b) the full field of the regression coefficients is contoured.

50 years of the integration (hereafter MODEL) when the surface meteorological variables were stored at intervals of three hours. The MODEL precipitation is verified for its interannual variability in relation to ENSO, against observed monthly total precipitation data from 4505 stations over South America (Webber and Willmott 1998, hereafter WW). It is available for a period of 30 years from 1960–90. The observed rainfall used for verification of the diurnal precipitation range in the MODEL is from the Tropical Rainfall Measuring Mission (TRMM) 3B42. This product is composed of 3-hourly-derived precipitation rates from 1998 to 2008 at horizontal resolution of 0.5°.

The seasonal mean diurnal precipitation range (used as one of the variables in the discussion of the results in the following section) is calculated as the seasonal average of the daily diurnal amplitude. A 3-hourly precipitation climatology is computed uniquely for each day of the December–February (DJF) season from the available period of TRMM and the MODEL simulation to derive a daily climatological diurnal cycle. This climatological diurnal cycle is used to fix the time of maximum and minimum precipitation for each day of the season. We then compute the seasonal diurnal range of precipitation for each year as the seasonal average of the daily precipitation difference between the time of maximum and minimum precipitation of this daily climatological diurnal cycle. Similarly, the diurnal range of the moisture flux convergence over the EA region is calculated as an area average of precipitation minus evaporation ($P - E$) from the MODEL and is computed as follows: A 3-hourly moisture flux convergence climatology is calculated uniquely for each day of the DJF season from the available period of MODEL simulation (i.e., 50 years) to derive its climatological diurnal cycle. Then the seasonal diurnal range of the moisture flux convergence is computed for each year as the seasonal average of the difference of the moisture flux convergence between the time of its maximum and minimum derived from the climatological diurnal cycle. The observed SST is from the Met Office Hadley Center Sea Ice and Sea Surface Temperature dataset (HadISST; Rayner et al. 2002).

3. Results

a. Precipitation

In Fig. 1a the precipitation anomalies obtained from regressing the mean DJF TRMM precipitation on the contemporaneous-observed Niño-3 (5°N–5°S, 150°–90°W) SST index (normalized by its standard deviation) is shown. The distinct precipitation anomalies over the EA and the anomalies with opposite sign over the Brazilian Highlands over the east coast are apparent in Fig. 1a.

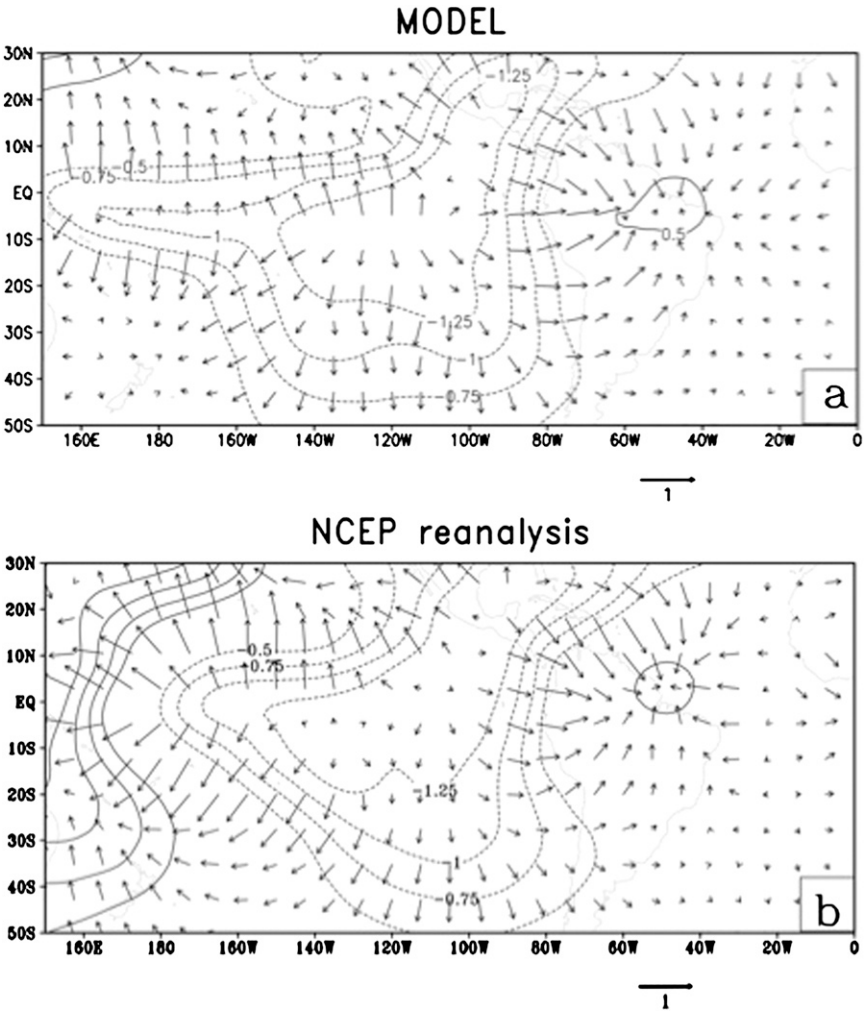

FIG. 3. The regression of the mean DJF velocity potential and divergent wind at 200 hPa on the corresponding standardized Niño-3 SST index from (a) MODEL and (b) NCEP–NCAR reanalysis. The unit of velocity potential (wind) is 1.0×10^{-6} m^2 s^{-1} (1 m s^{-1}, as shown by reference wind vector at bottom). The regressions correspond to 1σ of the Niño-3 SST index. Velocity potential significant at the 10% significance level according to t test is plotted; the full regressed field of the divergent wind is shown in both panels.

This teleconnection pattern over the EA from a relatively short observational record of TRMM dataset (10 years) used here is reasonably consistent with similar relationship obtained from a longer period of observed monthly total precipitation data from WW. The precipitation anomalies associated with the standardized Niño-3 SST index variations over the EA is quite consistent in both the TRMM and WW datasets. However, other regions of consistency of the ENSO teleconnection precipitation anomalies between the two precipitation datasets over a comparably larger area do not occur. The focus of this study is, however, centered over the EA region outlined in Fig. 1a where the two observational datasets are consistent. The corresponding MODEL result in Fig. 1c shows that the observed precipitation anomalies over the EA are reasonably well reproduced, whereas the anomalies are erroneously insignificant over southern South America. In addition, the precipitation anomalies in the MODEL over the Andes are contrary to that in the TRMM. It may be noted that the interannual precipitation anomalies in Figs. 1b and 1c persist even when the largest ENSO events (defined as when the Niño-3 SST index exceeds one standard deviation) is eliminated from the time series. This suggests that the interannual precipitation anomalies over the EA are quite robust.

Interestingly, it is found that both in the TRMM observations and in the MODEL, the interannual variations

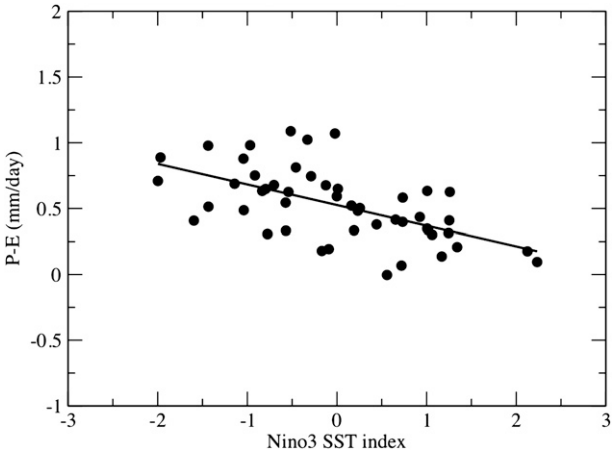

FIG. 4. The scatterplot from the MODEL of the mean DJF Niño-3 SST index with corresponding moisture flux convergence over the EA region (outlined in Fig. 1a). A least-squares fit line is also plotted, whose slope passes the *t* test at 90% confidence interval.

of the precipitation anomalies in the EA are also observed in the diurnal scales. This is shown in the regression of the mean DJF diurnal precipitation range on the corresponding standardized Niño-3 SST index from TRMM (Fig. 2a) and MODEL (Fig. 2b). The similarity in the regression pattern between the seasonal mean precipitation anomalies and the seasonal mean diurnal range anomalies of precipitation are apparent in both the TRMM and in the MODEL. This similarity suggests that the diurnal variations of precipitation over the EA are in some relationship with the remote ENSO forcing. Furthermore, Figs. 2a and 2b indicate that during warm (cold) ENSO events, the seasonal mean diurnal range of precipitation is decreased (increased) over the EA region. It may, however, be mentioned that the interannual variations of the diurnal range of precipitation in the MODEL is considerably weaker than TRMM (by nearly a factor of 4). Besides the errors in the COLA coupled climate model and its coarse horizontal resolution, it is also possible that the short record of the TRMM data could also be contributing to this difference. In a related study, Grimm and Tedeschi (2009) indicate from station observations that the highest sensitivity to ENSO seems to be in the extreme range of daily precipitation over an extensive region of South America, including that over the EA region.

b. The atmospheric bridge

The fundamental influence of ENSO variability on remote regional precipitation variability is from the shift in the large-scale atmospheric circulation patterns associated with the Walker (east–west) and Hadley (meridional) cells (Nigam 2003), apart from Rossby wave propagation from anomalous heat sources. This is shown in Fig. 3 as the regression of the mean DJF velocity potential and divergent wind at 200 hPa, both from the NCEP–NCAR reanalysis and the MODEL integration on the observed and MODEL standardized Niño-3 SST index, respectively. A 6-yr high-pass Butterworth filter is applied to the NCEP–NCAR reanalysis velocity potential and the HadISST datasets to remove variability on periods longer than the interannual time scales (Karspec and Cane 2002), so that the figure could be based on the same temporal scales as Fig. 1a. This filtering is especially important with the NCEP–NCAR reanalysis winds, because it is shown to exhibit an erroneous but significant interdecadal variability of the divergent circulation in the tropics (Kinter et al. 2004). The high-pass filtering of the MODEL simulation was found to be unnecessary as a result of insignificant interdecadal variations. Figure 3 suggests that the mean DJF upper-level divergence anomaly over the eastern Pacific during a warm ENSO event is associated with corresponding broad upper-level convergence over continental tropical South America. This observed anomalous atmospheric bridge in the NCEP–NCAR reanalysis is well simulated in the MODEL. This anomalous divergent wind pattern in both the NCEP–NCAR reanalysis and in the MODEL is centered over the EA region, which is consistent with the precipitation anomalies over the EA seen earlier in Figs. 1a and 1b.

c. Moisture flux convergence and surface evaporation

The roles of the two sources of moisture over the EA region—namely, moisture flux convergence and evaporation—is further analyzed in this subsection. It is seen that owing to the large-scale changes in the atmospheric circulation due to ENSO, the seasonal mean moisture flux convergence ($P - E$) over the EA region has a similar linear relationship with the Niño-3 SST index (Fig. 4) as in Fig. 1c. Essentially, Fig. 4 suggests that the moisture flux convergence over the EA increases (decreases) in the MODEL in cold (warm) ENSO events.

The question of how important a role is the land feedback playing in generating these interannual precipitation anomalies over the EA region in the MODEL is discussed here. In Fig. 5a the scatter between the lag of daily precipitation (averaged over the EA) with the corresponding daily evaporation (with the latter leading the former at positive lags) in the DJF season against the corresponding Niño-3 SST index from the MODEL is shown. These lags are computed from daily data of the MODEL simulation and are defined as the time (in days) when the correlation between the MODEL precipitation

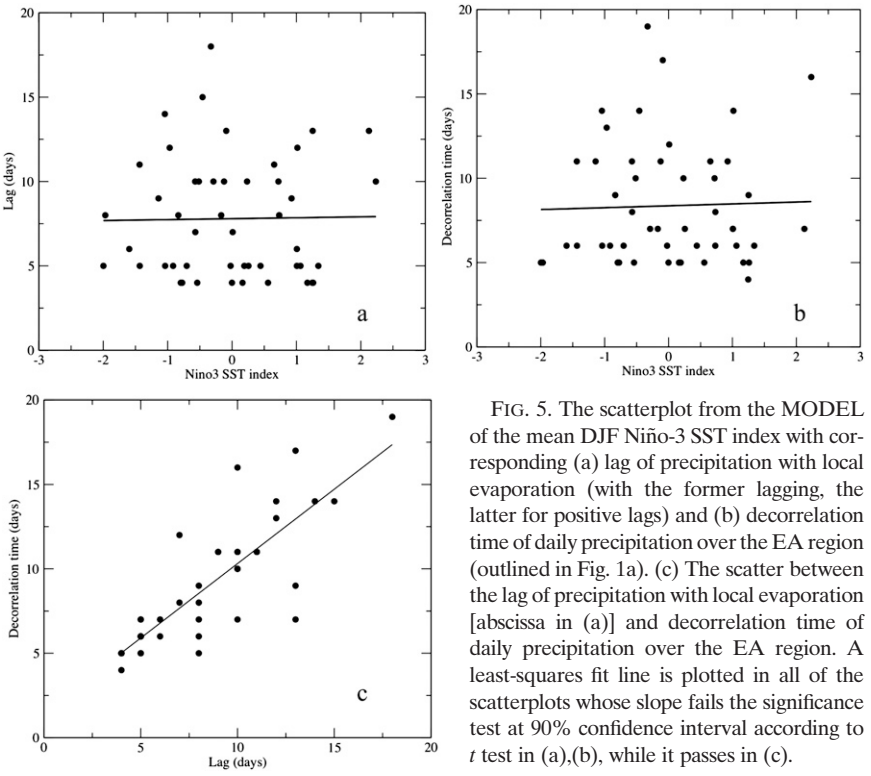

FIG. 5. The scatterplot from the MODEL of the mean DJF Niño-3 SST index with corresponding (a) lag of precipitation with local evaporation (with the former lagging, the latter for positive lags) and (b) decorrelation time of daily precipitation over the EA region (outlined in Fig. 1a). (c) The scatter between the lag of precipitation with local evaporation [abscissa in (a)] and decorrelation time of daily precipitation over the EA region. A least-squares fit line is plotted in all of the scatterplots whose slope fails the significance test at 90% confidence interval according to *t* test in (a),(b), while it passes in (c).

and evaporation falls below a significant value based on *t* test for 90 degrees of freedom. It is seen in the figure that there is an insignificant linear relationship between the lag of precipitation and evaporation with the Niño-3 SST index. It is equally important to notice that all the lags in Fig. 5a are positive. This suggests that the precipitation anomalies over the EA are sustained by local evaporation. Furthermore, the land feedback, as gauged by the lag between precipitation and evaporation over the EA region is relatively independent of the remote ENSO forcing. This can happen in regions where surface evaporation is not moisture limited (Guo et al. 2006).

Following Misra (2008a,b), an alternative strategy to diagnose land feedback is to look at the decorrelation time of the daily precipitation (defined as the time when autocorrelation trails below a significant value based on *t* test for 90 degrees of freedom). As Misra (2008a) indicates, the relatively long decorrelation time of the daily precipitation over the continental monsoon regions can be related to the robust land–atmosphere feedback. The decorrelation time in Fig. 5b, ranging from about 4 to 18 days from year to year over the EA, is well supported by the positive lags between evaporation and precipitation. That is, the relatively long memory of the daily precipitation over the EA is strongly sustained by the surface evaporation. This is supported by a strong linear relationship seen between the decorrelation time of daily precipitation and the lag between precipitation and evaporation over the EA shown in Fig. 5c. However, the lack of any significant linear relationship between the decorrelation time of the daily precipitation with the Niño-3 SST index reinforce once again that the local land–atmosphere interactions over the EA are relatively independent of the ENSO forcing. The panels in Fig. 5, therefore, collectively indicate that the local land–atmosphere feedback has weak interannual variations. This is partly because the region of the EA is not a moisture-limited region (Guo et al. 2006), especially in the austral summer season.

d. The amplification of the seasonal precipitation anomalies

In Fig. 6 we show the scatter of the DJF seasonal mean of the daily diurnal range of the moisture flux convergence over the EA from the MODEL against the corresponding Niño-3 SST index. The appearance of a rather strong linear relationship with the Niño-3 SST index in this figure provides evidence to suggest that the modulation of the moisture flux convergence at the diurnal scales over EA by the large-scale anomalous atmospheric bridge acts as a conduit to amplify the large-scale interannual variation of precipitation at the local diurnal scales.

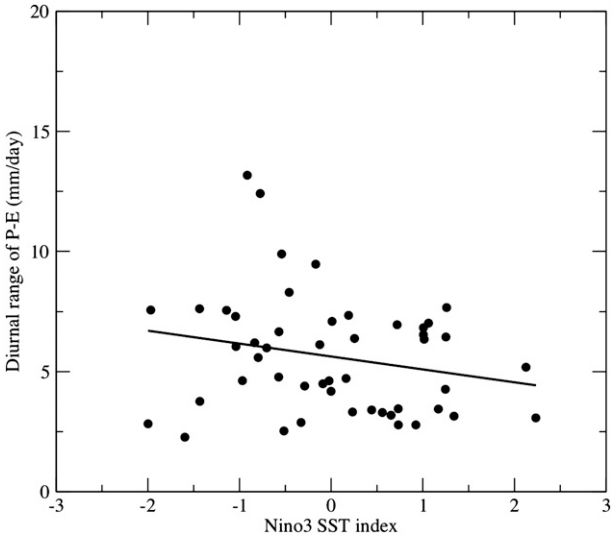

FIG. 6. Same as Fig. 4, but for diurnal range of $P - E$.

4. Conclusions

The EA region has a strong ENSO influence, as found in many of the previous studies. It is shown from this study that the amplification of the remote ENSO forcing is manifested on local diurnal variations. In this context it is worthwhile to recognize that the local diurnal variations exist independent of the ENSO variations. The fact that the remote ENSO signal manifests at local diurnal scales over the EA region suggests the importance of the diurnal variations to interannual variability. From a coupled model simulation that reasonably simulates the interannual variation of the EA precipitation, it is diagnosed that the interannual variation of the diurnal variations of the moisture flux convergence leads to corresponding variations in the precipitation. The land feedback is found to play a more passive role in sustaining these interannual precipitation anomalies over the EA while its role of maintaining long decorrelation times of daily precipitation in the region is acknowledged. It is recognized that this mechanism of local diurnal scales interacting with the large-scale interannual signal is primarily based on model results. The lack of a relatively long period of observations that also resolves diurnal variability in the area limits exhaustive verification of this proposed mechanism.

Acknowledgments. Thanks to the editor, Prof. William J. Gutowski, and three anonymous reviewers for their valuable comments on an earlier version of this manuscript. This research was supported by NOAA Grant NA07OAR4310268. The computing resources of the NASA Advanced Supercomputing (NAS) Division at Ames Research Center under Grant SMD-07-0382 are acknowledged.

REFERENCES

Bacmeister, J., P. Pegion, S. Schubert, and M. Suarez, 2000: An atlas of seasonal means simulated by the NSIPP-1 atmospheric GCM. Goddard Space Flight Center, NASA Tech Memo. 104606, Vol. 17, 194 pp.

Collins, W. D., and Coauthors, 2006: The Community Climate System Model Version 3 (CCSM3). *J. Climate,* **19,** 2122–2143.

Costa, M. H., and J. A. Foley, 2000: Combined effects of deforestation and doubled atmospheric CO_2 on the climate of Amazonia. *J. Climate,* **13,** 35–58.

Dirmeyer, P. A., and F. J. Zeng, 1999: Precipitation infiltration in the simplified SiB land surface scheme. *J. Meteor. Soc. Japan,* **77,** 291–303.

Enfield, D. B., and D. A. Mayer, 1997: Tropical Atlantic sea surface temperature variability and its relation to El Niño-Southern Oscillation. *J. Geophys. Res.,* **102,** 929–945.

Gent, P. R., and J. C. McWilliams, 1990: Isopycnal mixing in ocean circulation models. *J. Phys. Oceanogr.,* **20,** 150–155.

Giannini, A., J. C. H. Chang, M. Cane, M. A. Kushnir, and Y. Seager, 2001: The ENSO teleconnection of the tropical Atlantic Ocean: Contributions of the remote and local SSTs to rainfall variability in the tropical Americas. *J. Climate,* **14,** 4530–4544.

Grimm, A. M., 2003: The El Niño impact on the summer monsoon in Brazil: Regional processes versus remote influences. *J. Climate,* **16,** 263–280.

——, 2004: How do La Niña events disturb the summer monsoon system in Brazil? *Climate Dyn.,* **22,** 123–138.

——, and R. G. Tedeschi, 2009: ENSO and extreme rainfall events in South America. *J. Climate,* **22,** 1589–1609.

——, V. R. Barros, and M. E. Doyle, 2000: Climate variability in southern South America associated with El Niño and La Niña events. *J. Climate,* **13,** 35–58.

Guo, Z., and Coauthors, 2006: GLACE: The Global Land–Atmosphere Coupling Experiment. Part II: Analysis. *J. Hydrometeor.,* **7,** 611–625.

Hong, S.-Y., and H.-L. Pan, 1996: Nonlocal boundary layer vertical diffusion in a medium-range forecast model. *Mon. Wea. Rev.,* **124,** 2322–2339.

Kalnay, E., and Coauthors, 1996: The NCEP/NCAR 40-Year Reanalysis Project. *Bull. Amer. Meteor. Soc.,* **77,** 437–471.

Karspec, A. R., and M. A. Cane, 2002: Tropical Pacific 1976–77 climate shift in a linear, wind-driven model. *J. Phys. Oceanogr.,* **32,** 2350–2360.

Kiehl, J. T., J. J. Hack, G. Bonan, B. A. Boville, D. L. Williamson, and P. J. Rasch, 1998: The National Center for Atmospheric Research Community Climate Model: CCM3. *J. Climate,* **11,** 1131–1149.

Kinter, J. L., III, M. J. Fennessy, V. Krishnamurthy, and L. Marx, 2004: An evaluation of the apparent interdecadal shift in the tropical divergent circulation in the NCEP–NCAR reanalysis. *J. Climate,* **17,** 349–361.

Large, W. G., J. C. McWilliams, and S. C. Doney, 1994: Oceanic vertical mixing: A review and a model with a nonlocal boundary layer parameterization project. *Climate Dyn.,* **18,** 255–272.

Marengo, J. A., 1992: Interannual variability of surface climate in the Amazon basin. *Int. J. Climatol.,* **12,** 853–863.

——, and C. A. Nobre, 2001: The hydroclimatological framework in Amazonia. *The Biogeochemistry of the Amazon Basin,* M. E. McClaine, R. L. Victoria, and J. E. Richey, Eds., Oxford University Press, 17–42.

Misra, V., 2008a: Coupled interactions of the monsoons. *Geophys. Res. Lett.,* **35,** L12705, doi:10.1029/2008GL033562.

——, 2008b: Coupled air, sea, and land interactions of the South American monsoon. *J. Climate,* **21,** 6389–6403.

——, and L. Marx, 2007: Manifestation of remote response over the equatorial Pacific in a climate model. *J. Geophys. Res.,* **112,** D20105, doi:10.1029/2007JD008597.

——, and Coauthors, 2007: Validating and understanding the ENSO simulation in two coupled climate models. *Tellus,* **59A,** 292–308.

Moorthi, S., and M. Suarez, 1992: Relaxed Arakawa–Schubert: A parameterization of moist convection for general circulation models. *Mon. Wea. Rev.,* **120,** 1441–1467.

Nigam, S., 2003: Teleconnections. *Encyclopedia of Atmospheric Sciences,* J. R. Holton, J. Pyle, and J. A. Curry, Eds., Academic Press, 2243–2269.

Pacanowski, R. C., and S. M. Griffies, 1998: MOM3.0 manual. NOAA/GFDL Tech. Rep., 638 pp.

Paegle, N., and K. Mo, 2002: Linkages between summer rainfall variability over South America and sea surface temperature anomalies. *J. Climate,* **15,** 1389–1407.

Rayner, N. A., D. E. Parker, E. B. Horton, C. K. Folland, L. V. Alexander, D. P. Rowell, E. C. Kent, and A. Kaplan, 2002: Global analyses of sea surface temperature, sea ice, and night marine air temperature since the late nineteenth century. *J. Geophys. Res.,* **108,** 4407, doi:10.1029/2002JD002670.

Redi, M. H., 1982: Oceanic isopycnal mixing by coordinate rotation. *J. Phys. Oceanogr.,* **12,** 1443–1451.

Ronchail, J. G., G. Cochonneau, M. Molinier, J.-L. Guyot, A. Goretti De Miranda Chaves, V. Guimãraes, and E. de Oliveira, 2002: Interannual rainfall variability in the Amazon basin and sea-surface temperatures in the equatorial Pacific and the tropical Atlantic Oceans. *Int. J. Climatol.,* **22,** 1663–1686.

Ropelweski, C. F., and M. S. Halpert, 1987: Global and regional scale precipitation patterns associated with the El Niño/Southern Oscillation. *Mon. Wea. Rev.,* **115,** 1606–1626.

Slingo, J. M., 1987: The development and verification of a cloud prediction model for the ECMWF model. *Quart. J. Roy. Meteor. Soc.,* **113,** 899–927.

Smagorinsky, J., 1963: General circulation experiments with the primitive equations. I. The basic experiment. *Mon. Wea. Rev.,* **91,** 99–104.

Tiedtke, M., 1984: The effect of penetrative cumulus convection on the large-scale flow in a general circulation model. *Beitr. Phys. Atmos.,* **57,** 216–239.

Uvo, C. B., C. A. Repelli, S. E. Zebiak, and Y. Kushnir, 1998: The relationships between tropical Pacific and Atlantic SST and northeast Brazil monthly precipitation. *J. Climate,* **11,** 551–562.

Webber, S., and C. J. Willmott, 1998: South American precipitation: 1960-1990 gridded monthly time series. Station records archive (version 1.02). [Available online at http://climate.geog.udel.edu/~climate/html_pages/README.sa.p.ts.html.]

Xue, Y. K., P. J. Sellers, J. L. Kinter III, and J. Shukla, 1991: A simplified biosphere model for global climate studies. *J. Climate,* **4,** 345–364.

——, F. J. Zeng, and C. A. Schlosser, 1996: SSiB and its sensitivity to soil properties—A case study using HAPEX-Mobilhy data. *Global Planet. Change,* **13,** 183–194.